Quantitative Inspection of Internal Raster Orientation of Additively Manufactured Components via Ultrasonic Nondestructive Testing

Atik Amin, David Jack, Trevor Fleck
Department of Mechanical Engineering, Baylor University, 1301 S University Parks Dr, Waco, TX, 76798

Abstract

This paper quantifies the internal raster pattern of an additively manufactured component using high-resolution ultrasonic imaging method. Research has demonstrated that final part performance is a function of the internal raster patterns for each layer. This paper presents a method using ultrasonic nondestructive testing to quantify these internal raster patterns, giving insights into component performance. The polymers used in this study include poly cyclohexylenedimethylene terephthalate glycol (PCTG), carbon fiber-filled polyethylene terephthalate (PET-CF), and a high temperature grade nylon (HTN). These materials were selected based on their representation of a wide variety of uses in the industry for producing automotive parts, biomedical equipment, conveyer and seat belts, threads, nets and ropes. In this work a method utilizing immersion ultrasonic testing (UT), with a 10 MHz spherically focused transducer, is presented to investigate 3D printed components manufactured with various raster orientation sequences. An in-house MATLAB script was developed to analyze the UT Data, with the objective of quantifying the internal raster pattern. Using this script, C-Scan images from each layer of each sample is extracted. These extracted images are then used to measure the raster orientation through a manual approach, where points across the individual raster are used to quantify the orientation. Results show that the method is successful in capturing the proper orientation state at least for the first 9~10 layers of PCTG and PET-CF and for HTN samples the method was successful up to 18th layer for the first two orientation patterns and 16th layer for the last orientation pattern afterwards the return signal attenuates, making accurate quantification challenging. The results extracted from the method used in this experiment showed errors between 2-4 degrees. Results are presented to show the sensitivity of the method to variations in material systems. The results of this paper provide insight into the effect of material on the attenuation of ultrasonic waves in AM components, which will dictate the feasibility of using UT to inspect similar AM components.

Keywords: Additive Manufacturing, Raster Orientation, Ultrasonic Nondestructive Testing, Fused Filament Fabrication

Background

Due to the increasing demand and cost effectiveness, additive manufacturing (AM), also known as 3D printing, has become a popular technique for manufacturing objects consisting of polymers, ceramics, or metals. AM offers several advantages over traditional methods of manufacturing such as ease of producing components with complex features, as well as the ability to produce custom components with tailored performance [1]. Among the most popular of the main AM techniques, fusion-based material extrusion methods, or more popularly known as fused deposition modeling (FDM) or fused filament fabrication (FFF), is used because of its unique capability of extruding material in a layer-by-layer manner to achieve the custom, complex geometries previously mentioned. In FFF processes, material extrusion is achieved by melting a filament in a heated nozzle and depositing the molten layers onto previously deposited layers.

The deposited layer then rapidly cools and solidifies to provide the expected shape [2]. The most common polymers in FFF processes are acrylonitrile butadiene styrene (ABS) and polylactic acid (PLA) [3] but these two materials are not widely used in the industry as they lack many of the required functional characteristics. PLA has a relatively low glass transition temperature that makes it unsuitable for high temperature applications. The chemical resistance of ABS makes it an unreliable product for industrial purposes and when burnt, it generates high smoke that causes air pollution and at the same time it is toxic as well. High temperature nylon (HTN) is a well-suited material for applications requiring a higher melting point. The main purpose of using HTN is its heat resistance, allowing it to be used for under the hood applications in the automotive industry. PCTG is a co-polyester and well suited for applications requiring high stability and high impact. PET-CF is generally used for smooth surface finish, improved mechanical properties, and increased heat resistance capability (up to $100^{O}C$).

Raster orientation is typically defined as the direction of the individually deposited beads during the FFF process. The overall mechanical properties of an FFF component's strength is highly dependent on the orientation of these printing paths. There are numerous process parameters, such as layer thickness, raster width, print direction, nozzle temperature and so on; all of which are known to play a significant role in for maintaining the structural properties and the resultant bond strength [4]. According to Pandey et. al. the raster orientation plays a significant role due to its effect on build time, dimensional accuracy, and support structure [5]. They have also mentioned that orientation is an essential factor for part strength, precision, layer deposition time and cost in layered manufacturing systems. Several other researchers studied the effect of raster orientation on the internal properties of a 3D printed part manufactured with ABS [6]. Wu et al. have indicated in their experiments that raster angles can exhibit great impact in assessing the mechanical strength of an additively manufactured part [7]. Moreover because of the weak inter layer bond strength, test samples containing 0^{o} orientation were raptured at individual layer steps. It was also believed phase change might occur when a semi molten filament extrudes and solidifies in a chamber. As a result, material contraction is likely to happen causing unstable interlayer connection and high permeability [8].

In terms of ultrasonic nondestructive testing, there have been several efforts shown in literature to date. The significance of ultrasonic testing on a 3D printed part has been discussed in the works of Camineroa et. al. [9], where the ability to detect barely visible impact damage is investigated. Another experiment investigated high-frequency phased array ultrasonic testing (PAUT) methods to check relationship between the gap width and tensile properties of a 3D printed part [10]. Prior to their experiment the defects within the part were intentionally fabricated and the images extracted after the ultrasonic test exhibited distinguishable defected zones within the specimen. The measured gap width was found significantly smaller than the designed value with an error below 10%. The present study is done to investigate the internal pattern of a 3D printed component to verify the accuracy of the developed method of immersion test. The manual procedure of selecting individual points within the rasters and measuring the slope made it convenient for the users to verify the print direction of the 3D printer used in the experiment.

Research Methodology

In this section, the procedures followed while processing the experimental works will be discussed. Process parameters such as selection of materials, nozzle size, transducer frequency, layer height etc. were chosen before beginning the experiment. The developed MATLAB script is used to turn the ultrasonic scan data into C-Scan results to inspect the number of layers and the raster orientation.

Material Selection

The work here was completed using an industrial-scale FFF printer (Essentium HSE 180 HT) capable of achieving high quality prints using the functional materials relevant for industrially applications, with a nozzle diameter 0.8mm. The parts used in the present study are 3-inch x 3-inch with a thickness of 0.25 inch. For the immersion tank ultrasonic testing, only one transducer having a frequency of 10 MHz was selected to investigate three different samples prepared with varying raster orientations. The CAD model of the part was prepared and sliced into gcode instructions for the printers using the commercial slicing software (Simplify 3D). The three different polymers selected were PCTG, PET-CF, and high-temperature nylon (HTN). A layer height of 0.35 mm was used, resulting in an 18-layer thick component. For each material, three different samples containing different raster orientations were prepared. The orientation patterns for each material parts were assigned and marked as Part A, Part B and Part C that refer the materials PCTG, PET-CF and HTN respectively. All these parts contained three different raster orientation patterns (e.g., A1, A2, A3, B1, B2, B3 etc.) ending up to nine total samples, across the three materials. The first raster orientation pattern used was [0 90 ,10 100 ,20 110, 30 120, 40 130, 50 140, 60 150, 70 160, 80 170] for parts A1, B1 and C1. Each pair of the A1, B1 and C1 parts were printed with 90^{o} angular increments to reduce warping during the print. The raster orientations [0 60 120 20 80 140 40 100 160 60 120 180 80 140 200 100 160 220] were assigned to Parts A2, B2 and C2. For Parts A3, B3 and C3 no particular pattern sequence was followed, as in patterns 1 and 2, in order to “randomize” the detectability, using orientations of [0 90 45 135 20 110 70 160 50 140 85 175 25 115 10 100 110 180].

Figure 1 shows the immersion system tank along with test samples prepared with PCTG, PETCF, and HTN. A representative PCTG coupon is shown within the immersion tank, directly below the ultrasonic transducer which can raster across the part as shown in Figure 3. The part was placed in a 3D printed holder that allowed for easy alignment of the samples. The other two parts in Figure 1 are shown with a measuring scale that verifies the dimension used for printing the parts.

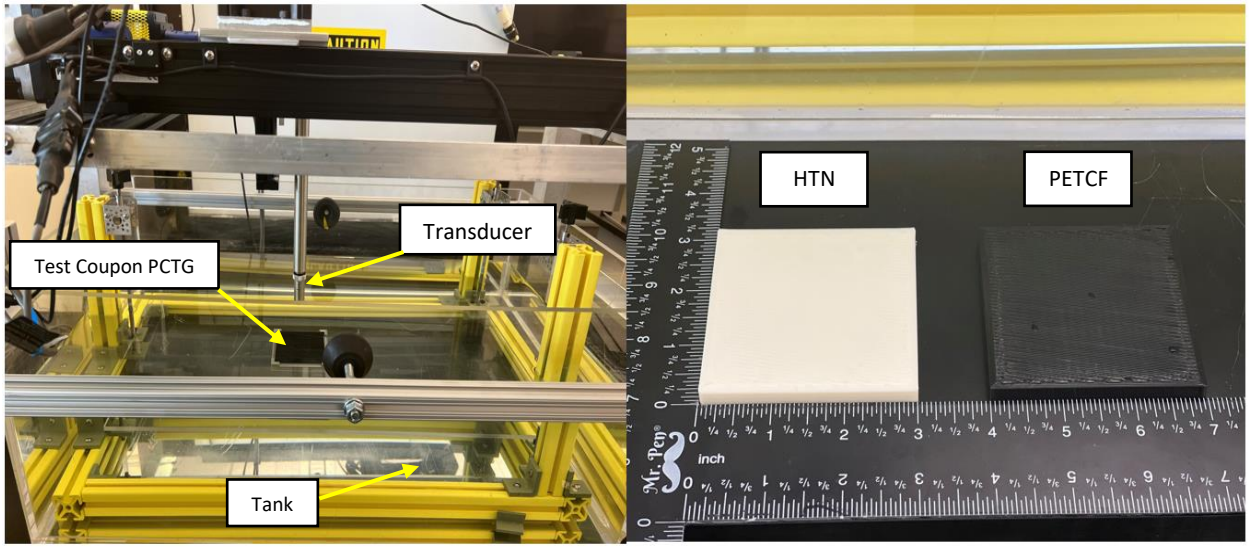

Figure 1: Immersion System Tank Test samples (a) PCTG (b) PETCF (c) HTN

Experimental Setup

The immersion system tank was used to perform the ultrasonic testing, which used a transducer with a frequency of 10MHz. A representative A-Scan signal that transmitted through the 3D printed PCTG component approximately within 6.5μs can be seen in Figure 2. The sharp peak at the end of the signal in Figure 2 indicates the signal has reached the back wall of the part. To get a better visibility of the deposited layers, the transducer signal was focused on the middle of the part. All scans were performed with a resolution of 0.1 mm. The scan process consisted of rastering the transducer over the immersed test sample to acquire A-scans (such as that shown in Figure 2) at various locations on the part. These A-scans were then accumulated using a custom MATLAB script to produce a 3D data set. The individual layer images for a given depth are collected from the C-Scan corresponding to that given depth, and the angular measurement of individual raster was obtained using a manual approach from the resulting C-Scan. For this experiment, a 40 mm by 40 mm area within the test specimen was scanned, with the raster path shown in Figure 3.

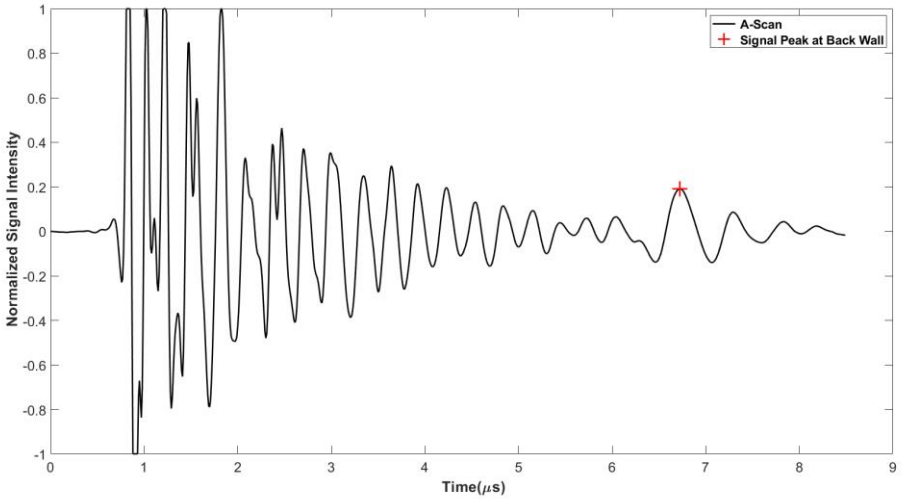

Figure 2: A Scan image for at (X_{index}, X_{scan}) = (25mm, 25mm) from Part A-1 using a 10 MHz Transducer

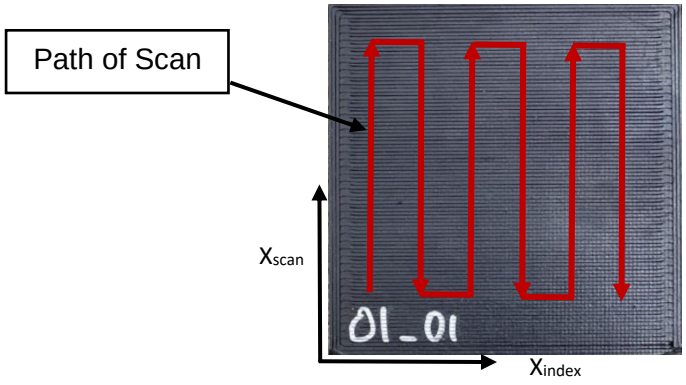

Figure – 3: Path of Ultrasonic Scan

Analysis and Results

A MATLAB script was used to generate the images of the C-Scan at each representative depth. Individual layer images are plotted and a manual approach of selecting two points was performed to quantify the of the raster orientation. After completing the measurement process, each layer was matched to their respective print pattern of the test samples, as sliced using the commercial software, Simplify3D. Figures 4 and 5 exhibit how the raster orientations at 3rd & 10th raster layers into the parts look like for the three different material systems used in the experiment orientation pattern 01.

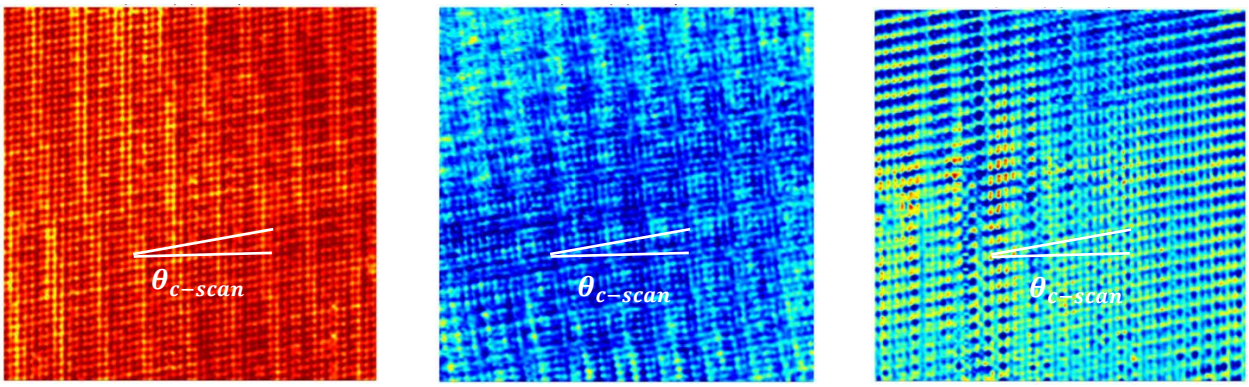

(a) (b) (c)

Figure 4: Raster Orientation of 3rd Layer of Pattern 01 Extracted from C-Scan (a) PCTG (b) PETCF (c) HTN

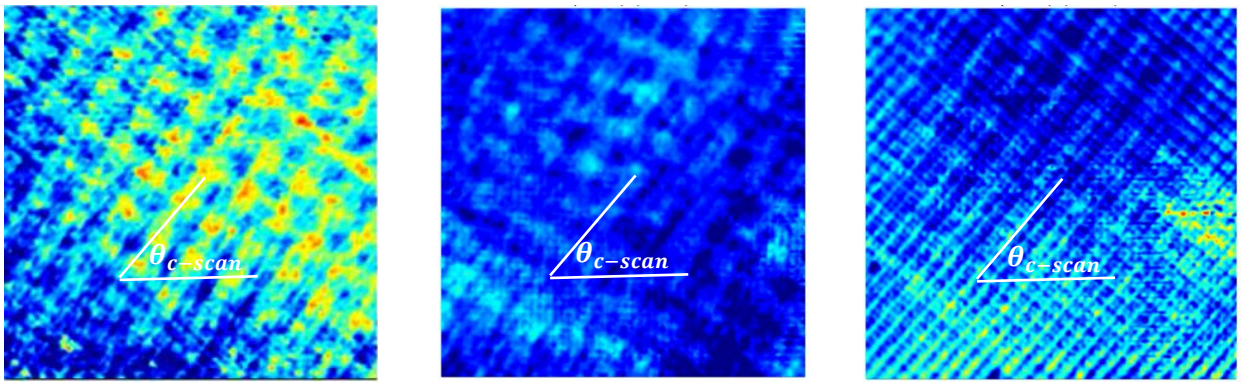

(a) (b) (c)

Figure 5: Raster Orientation of 10th Layer of Pattern 01 Extracted from C-Scan (a) PCTG (b) PETCF (c) HTN

From the resulting C-Scans we select visible lines (rasters) from a layer and select two points in a single line selected. The manually selected point values from the individual rasters were used to measure slopes, and then used to calculate the orientation angle. The two points in a line were selected three times for each layer and every time the considered lines were different. The values of slopes as well as the raster angles were measured three times, with the points being taken from different visible rasters at top, middle and bottom of each layer. From the slope the

orientation of a raster in a particular layer was measured for each three selection and the average of these values was compared with the originally designed orientation. The differences between the actual and measured values were calculated in degrees and finally the deviations were plotted for each pattern of rasters in Figure 6, with the equations for the slope and orientation angle being:

$$m = \frac{y(2)-y(1)}{x(2)-x(1)} \tag{1}$$

$$\theta = tan^{-1}(m) \tag{2}$$

The Figure 6(a) refers to the plots of designed and measured orientations and Figure 6(b) represents the errors against the layer numbers for three different orientation patterns of PCTG, PET-CF and HTN. The measured orientations shown in Figure 6 (a) is accomplished by calculating the average of the raster angles in each layer. It is evident that in Figure 6 (a) at least 10 layers can be seen properly for each material system and soon after the 10th layer the visibility started to decrease for PET-CF. There are a few layers after the 10th layer in PCTG of pattern 01 visible but the chances of seeing the raster orientations properly are negligible as it might provide huge errors. In Figure 6 (b) the errors are measured by following the equation (3). The mathematical difference between the originally designed and measured orientations is taken instead of relative difference for easily understanding the deviation. Another reason was the values of relative differences in in each layer are too small as the errors in each visible layers remained within 2-4 degrees for each material used in the experiment.

$$Error = \left|\theta_{\text{designed}} - \theta_{\text{measured}}\right| \tag{3}$$

The pattern 01 denoted in Figures 06 refer to the raster orientations [0 90 ,10 100 ,20 110, 30 120, 40 130, 50 140, 60 150, 70 160, 80 170], have been assigned to the parts A1 for PCTG; B1 for PET-CF; C1 for HTN consecutively. Similarly in Figure 7 the pattern 02 represents the raster orientations [0 60 120 20 80 140 40 100 160 60 120 180 80 140 200 100 160 220] and relegated to the parts A2 for PCTG; B2 for PET-CF; C2 for HTN. The parts A3 for PCTG; B3 for PET-CF; C3 for HTN are comprised of the third orientation pattern shown in Figure 8.

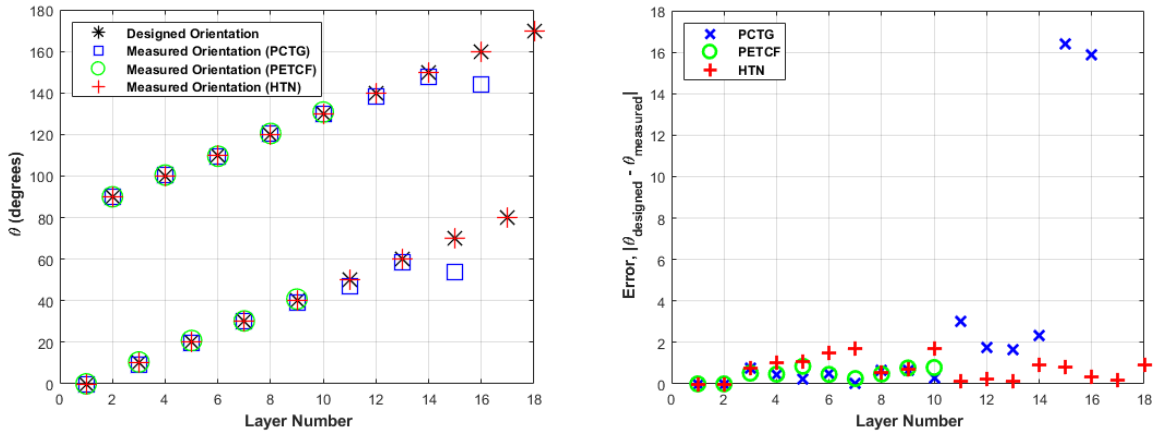

(a) (b)

Figure 6: Plots of measured orientations and errors of three material systems (Pattern 01)

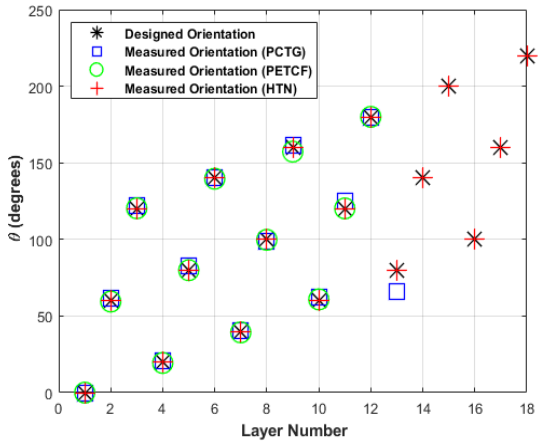

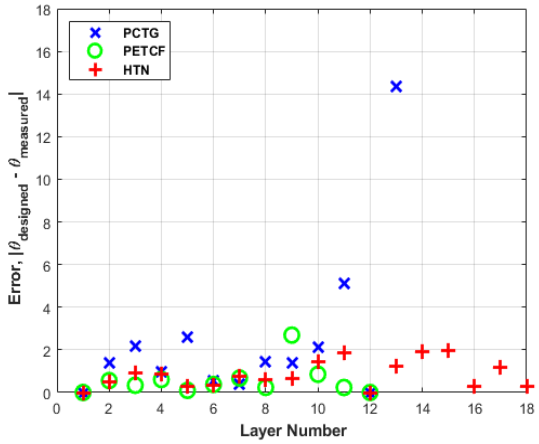

(a) (b)

Figure 7: Plots of measured orientations and errors of three material systems (Pattern 02)

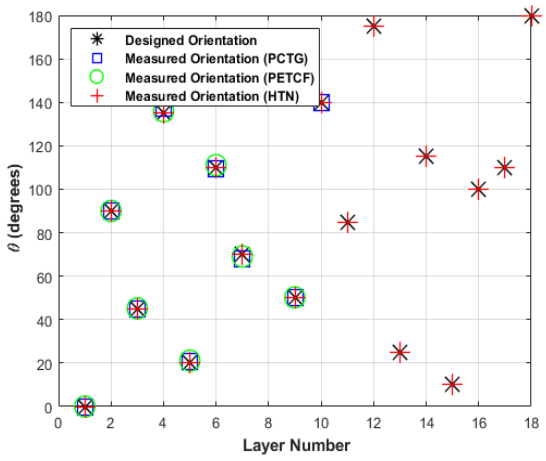

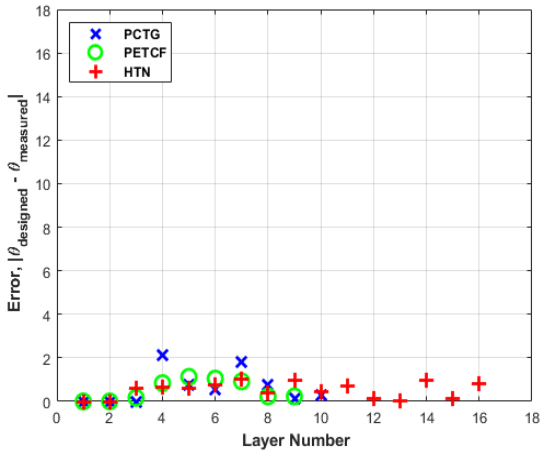

(a) (b)

Figure 8: Plots of measured orientations and errors of three material systems (Pattern 03)

Among all the materials used, HTN showed the best results, with Parts A1 and B1 being visualized for all 18 layers. The last orientation pattern showed 16 properly visible layers after the ultrasonic test. The investigation demonstrates that HTN did had clearer images as compared to PET-CF and PCTG as can be seen from Figure 4 and Figure 5. This resulted in higher accuracy of layer measurement as all three parts printed with HTN could be seen through up to at least 16 layers whereas all other test specimens of PCTG and PET-CF exhibit only 9-10 measurable layers properly. The reason for the higher accuracy seen in the HTN samples will be a subject of future study. In case of PCTG, fewer than 10 layers could be accurately measured with the rasters not being visible after the 13th layer due to signal attenuation, particularly seen in patterns 02 and 03. One probable reason might be the pairs or groups of orientation patterns that distinguish all three test coupons of PCTG. Pattern 03 has irregular orientation pairs, and this could be one reason for the early signal attenuation whereas patterns 01 and 02 have synchronized sets of groups that might have caused the signal to pass through the material better than randomly oriented layers.

Conclusion

Detecting and analyzing the internal mechanical properties of a thermoplastic being produced via AM is important for maintaining the quality of 3D printed part. The present work is also used as a measure of determining the feasibility of assessing the quality of FFF components using ultrasonic nondestructive testing. The work described in this article lays the foundation for the inspection of FFF components. In this experiment it is observed that the material system of HTN showed better performance than PCTG & PET-CF and almost all the layers could be seen properly. Apart from HTN, other materials exhibited almost 9~10 layers properly and a few more layers after the 10^{th}. The angular measurements from the properly visible layers were almost accurate and the error remained within 2-4 degrees. The present study is done only with a 10 MHz transducer, but a more extended work can be done with a range of transducers having different frequency levels. Moreover, instead of using three different orientation patterns for three parts of a single material system more parts can be included to find the standard deviation. Future work will include automation of the raster orientation process and examining bigger parts manufactured with additive manufacturing process. Additionally, X-Ray Computed Tomography machine could be explored for validation purposes.

Bibliography

1. D. Jiang, D.E. Smith, “Anisotropic mechanical properties of oriented carbon fiber filled polymer composites produced with fused filament fabrication” Addit. Manuf.18 (2017) 84–94, https://doi.org/10.1016/j.addma.2017.08.006.
2. T.J. Coogan, D. O. Kazmer, “Prediction of interlayer strength in material extrusion additive manufacturing” 2020, https://doi.org/10.1016/j.addma.2020.101368
3. A. Kantaros, D. Karalekas, “Fiber Bragg grating based investigation of residual strains in ABS parts fabricated by fused deposition modeling process”, Mater. Des.50 (2013) 44–50, https://doi.org/10.1016/j.matdes.2013.02.067.
4. Sood A.K., Ohdar R.K., Mahapatra S.S., “Parametric appraisal of mechanical property of fused deposition modelling processed parts” Mater Des 2010;31(1):287–95.
5. Pandey P.M., Venkata Reddy N., Dhande S.G., “Part deposition orientation studies in layered manufacturing” J Mater Process Technol 2007;185:125–31.
6. Durgun, I.; Ertan, R., Experimental investigation of FDM process for improvement of mechanical properties and production cost. Rapid Prototyp. J. 2014, 20, 228–235.
7. W. Wu, P. Geng, G. Li, D. Zhao, H. Zhang, J. Zhao, “Influence of layer thickness and raster angle on the mechanical properties of 3D-Printed PEEK and a comparative mechanical study between PEEK and ABS”, Materials 8 (2015) 5834–5846, https://doi.org/10.3390/ma8095271.
8. Es-Said O.S., Foyos J., Noorani R., Mandelson M., Marloth R., Pregger B.A., “Effect of layer orientation on mechanical properties of rapid prototyped samples”, Mater Manuf Process 2000;15:107–22.
9. M.A. Camineroa, I. García-Morenoa, G.P. Rodrígueza, J.M. Chacónb, “Internal damage evaluation of composite structures using phased array ultrasonic technique: Impact damage assessment in CFRP and 3D printed reinforced composites”, 2018.
10. K. Fayazbakhsh, F. Honarvar, H. Amini, A. Varvani-Farahani, “High frequency phased array ultrasonic testing of thermoplastic tensile specimens manufactured by fused filament fabrication with embedded defects”, 2021.
11. J.K. Na, E.K. Oneida, “Nondestructive evaluation method for standardization of fused filament fabrication based additive manufacturing”, Addit. Manuf. Article 24 (2018) 154–165, https://doi.org/10.1016/j.addma.2018.09.024.

12. Y. Jin, E. Walker, H. Heo, A. Krokhin, T.-Y. Choi, A. Neogi, “Nondestructive ultrasonic evaluation of fused deposition modeling based additively manufactured 3D-printed structures”, Smart Mater. Struct. 29 (4) (2020) 045020
13. Y.L. Yap, et al., “A non-destructive experimental-cum-numerical methodology for the characterization of 3D-printed materials—polycarbonate-acrylonitrile butadiene styrene (PC-ABS)”, *Mech. Mater.* Article 132 (2019) 121–133, https://doi.org/10.1016/j.mechmat.2019.03.005.
14. M.A. Caminero, I. Garcia-Moreno, G.P. Rodriguez, J.M. Chacon, “Internal damage evaluation of composite structures using phased array ultrasonic technique: Impact damage assessment in CFRP and 3D printed reinforced composites”, *Compos. B Eng.* Article 165 (2019) 131–142, https://doi.org/10.1016/j.